Available online at www.sciencedirect.com

ScienceDirect

Chinese Journal of Aeronautics 23(2010) 623-630

Chinese Journal of Aeronautics

www.elsevier.com/locate/cja

A Passive Method to Control Combustion Instabilities with Perforated Liner

Li Lei, Guo Zhihui, Zhang Chengyu, Sun Xiaofeng*

School of Jet Propulsion, Beijing University of Aeronautics and Astronautics, Beijing 100191, China

Received 12 October 2009, accepted 29 June 2010

Abstract

The effectiveness of perforated liner with bias flow on the control of combustion instability is investigated. Combustion instabilities result from the coupling between acoustic waves and unsteady combustion heat release. Sometimes the phenomenon happens in afterburners of aeroengine and rocket engine, and it always causes damage to flame holders, liner sections and other engine components. Passive methods, such as perforated liner, are often used to suppress such instabilities in application. In this article, first, a burner testbed is built in order to study the characteristic of this phenomenon. The unstable frequencies and unstable area are investigated experimentally. Then an analytical model, based on "transfer element method", is developed and the numerical results are compared with those from experiments. At last the perforated liner is applied to the burner to suppress the instabilities. The results show that the sound pressure can be greatly reduced by the perforated liner.

Keywords: combustion instabilities; combustors; perforated liner; bias flow; resonating frequency

1. Introduction

In gas turbine lean premixed prevaporised (LPP) combustion is used by mixing the fuel and air more evenly before combustion for low NO_x emissions. This means that the combustors are highly susceptible to combustion instabilities. Combustion instabilities are self-excited oscillations due to the interactions between combustion and sound waves. One of the natural acoustic modes of combustor is excited by unsteady heat release, and then it will enlarge the unsteady heat release. Then a feedback loop in combustion process is formed, which sometimes results in large and damaging oscillations [1].

Combustion instabilities are often suppressed by either active or passive methods. Active control techniques always involve a complex control system and the actuator. For example, M. A. Heckl controlled the noise from an electrical Rijke tube using loudspeaker as the actuator[2]. And the control of combustion oscillations with a high-momentum air-jet was studied by J. H. Uhm, et al.[3]. These active control methods really offer the potential to readjust a combustion system to accommodate problems like changing ambient conditions or fuel composition. However the instabilities always occur in a very short time, and it is difficult to design a complex implement system in industrial application.

Currently, in most practical combustors, the passive methods are widely used, which add acoustic damping to the combustion system. Helmholtz resonators and perforated liners are two particular passive control devices. The absorption of the Helmholtz resonator and side branch resonator to the sound energy in a thermoacoustic system was investigated by I. D. J. Dupere, et al.[4] , who gave the design criteria about the parameters of Helmholtz resonator, such as neck length, size of aperture, the chamber volume and position in the whole system. Tuned control was done by D. Zhao, et al.[5], in the way of varying the area of Helmholtz resonator neck. However, the Helmholtz resonator usually has a too large body to be used in compact places such as aeroengine.

The cooling flow system in modern combustor can be simplified as perforated plate with bias flow, which has been pointed out by J. D. Eldredge, et al.[6]. The absorption of acoustic waves by this form of liner has also been studied by X. D. Jing, et al.[7-8] and J. D. Eldredge, et al.[6,9], which provides theoretical basis for using perforated liner for controlling the combustion instabilities. But in these works, the unsteady heat re-

*Corresponding author. Tel.: +86-10-82317008.
E-mail address: sunxf@buaa.edu.cn
Foundation items: National Natural Science Foundation of China (50890181); Aeronautical Science Foundation of China (2009ZB51)

doi: 10.1016/S1000-9361(09)60263-6

lease is not included so the effects of the perforated liner on the instabilities in a combustion system could not be accurately investigated. It is still a problem to calculate the resonating frequencies of the system including a heat release model and the perforated liner.

Helmholtz resonator can be treated as lumped parameter system, the effect of which can be investigated in a one-dimensional (1D) mathematical model. But perforated liner is a distributed parameter system, so three-dimensional (3D) model, which can include unsteady heat release model and the impedance wall boundary conditions, is needed. Our work is based on the 3D linear stability analysis developed by D. N. You, et al.[10]. What's more, the direct method for treating liner would bring us a double iteration process for the calculation of the wall compliance and the frequency and it would bring large difficulties to numerical methods. Thus some feasible approaches are needed to describe the effect of the liner. Fortunately a method called "transfer element method (TEM)", based on equivalent surface source method[11-12], has been used and then the double iteration calculation process is avoided.

In this article, firstly, experiments of simple premixed prevaporised methane-fueled combustor are introduced. In the experiments the large oscillations occur when equivalence ratio changes from 0.6 to 0.9. The perforated liner is used for the instabilities damping. Secondly, an analytical 3D model is established which includes the effect of perforated liner and the heat release model. Finally, the experimental results are compared with the model prediction results.

2. Experimental Setup

A middle-pressure air source which can provide a quiet air supply is used for the combustion experiments. The storage vessels hold sufficient air for a constant pressure supply under the typical running conditions for at least 1 h. The air pressure in the rig is controlled by air reducing valve. The air comes into the premixed section from a sonic inlet. Then upstream disturbances cannot propagate to experimental part. And it can also provide a well-defined isentropic boundary condition at the upstream end (see Fig.1). The methane is supplied in the premixed section, so the disturbances from combustor can infect the fuel flow rate.

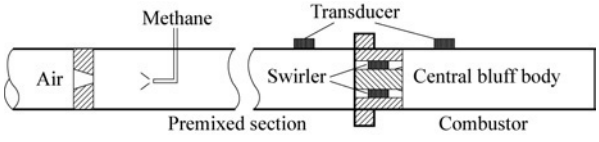

Fig.1 Experimental setup.

The premixed part is a cylindrical duct of 80 mm in diameter and 1 500 mm in length. There is a pressure transducer located at the place of 360 mm far away from the combustor in the duct. The combustor is also a cylindrical duct, whose outer diameter is 89 mm, inner diameter is 77 mm and length is 540 mm. For the combustor part, the rigid wall can be changed into perforated plate with back chamber, which provides damping to the whole system. There is a central bluff body between the premixed section and the combustor. The central bluff body is of 30 mm in diameter and the outer diameter is 40 mm. There is a swirler in the nozzle and the swirler number in our experiments is 0.83.

The air flow rate is kept at 16 g/s. When the methane equivalence ratio is 0.55, the mixed gas begins combusting. But the flame is not stabilized on the central bluff body and swings in the combustor. The disturbance pressure is small, so the combustion is stable. When the equivalence ratio is increased to 0.62, the intermittent instability occurs and some clear resonating pressure signals can be gathered. When the equivalence ratio is larger than 0.7, large disturbances occur. The max pressure fluctuation can be more than 10 kPa (see Fig.2)

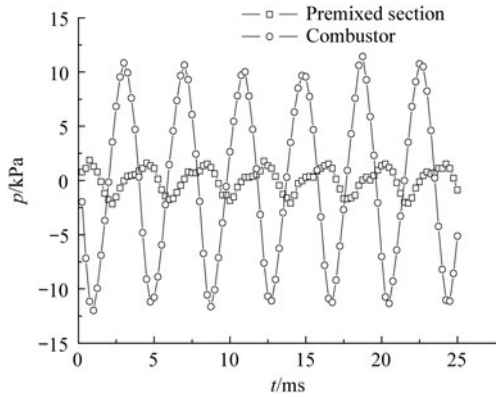

Fig.2 Part of fluctuation pressure in time domain in combustor and premixed section.

In order to control the large fluctuation, perforated liners of different parameters will be located at the downstream area of the flame. When combustion instability occurs, the flame is almost in the 100 mm area after the bluff body. The perforated liner is 140 mm away from the bluff body. Then the cool bias flow from the perforated plate would not infect the flame.

3. Analytical Model

A 3D linear stability analysis, which could be used to treat a broader class of problems involving complicated configurations and non-uniform flow distributions in gas turbine combustors, was developed by D. N. You, et al.[10]. We simply introduce it first. In the cylindrical coordinates, velocity, pressure and density, which are denoted by $\bar{u}$, $\bar{p}$, and $\bar{\rho}$ respectively, are decomposed into a time-mean value and a small perturbation quantity:

$$\bar{p}(\boldsymbol{r},t) = p_0(\boldsymbol{r}) + \tilde{p}(\boldsymbol{r},t) \quad (1)$$

where p_0 is the time-mean value of pressure, $\tilde{p}$ the

small perturbation quantity of pressure, $\boldsymbol{r}$ the coorclinate vector.

The same is true of velocity and density variables. Thus the conservation equations are linearized, and wave equation can be derived. A circular duct is divided into a number of cells along the axial direction, which are denoted by $j-1$, j, $j+1$, ⋯. The cross-sectional area and axial distributions of mean flow properties are assumed to be uniform within each cell. Then the solution of the wave equation for each cell has the following form:

$$\tilde{p}^{j}(x,\theta,r,t)=\sum_{m=-\infty}^{+\infty}\sum_{n=1}^{\infty}(P_{mn}^{+j}\psi_{mn}^{+j}(r)\mathrm{e}^{\mathrm{i}\alpha_{mn}^{+j}(x-x^{j})}+P_{mn}^{-j}\psi_{mn}^{-j}(r)\mathrm{e}^{\mathrm{i}\alpha_{mn}^{-j}(x-x^{j})})\mathrm{e}^{\mathrm{i}(m\theta+\omega t)} \quad (2)$$

where x, θ, r stand for the position variables of axial, circumferential and radial directions respectively, P is the unknown parameter, and ψ is the radial eigenfunction; the subscripts m and n denote the circumferential direction mode number and the radial direction mode number, respectively; α is the axial wave number; "+" and "–" denote the waves that propagate upstream and downstream, respectively; and ω is the complex parameter, for which $\omega=\omega_{\mathrm{r}}+\mathrm{i}\omega_{\mathrm{i}}$; the real part ω_{r} denotes the real resonating frequency, and the imaginary part ω_{i} determines the growth rate of a particular acoustic mode. If $\omega_{\mathrm{i}}>0$, the energy dissipation is more than the energy gaining, and the system is stable. If $\omega_{\mathrm{i}}<0$, the system is unstable, and it will cause large fluctuation for pressure and velocity.

The velocity and the density oscillation have the same form as pressure waves. According to the conservation law of mass, momentum and energy, the oscillatory flow-fields are matched in adjacent cells. Then following equations can be obtained:

$$\sum_{n=1}^{\infty}[\psi_{mn}^{+j}(r)P_{mn}^{+j}+A_{mn}^{-j}\psi_{mn}^{-j}(r)P_{mn}^{-j}+A_{\mathrm{v}mn}^{+j}\psi_{\mathrm{v}mn}^{+j}(r)\rho_{\mathrm{v}mn}^{+j}+A_{mn}^{+j+1}\psi_{mn}^{+j+1}(r)P_{mn}^{+j+1}+A_{mn}^{-j+1}\psi_{mn}^{-j+1}(r)P_{mn}^{-j+1}+A_{\mathrm{v}mn}^{+j+1}\psi_{\mathrm{v}mn}^{+j+1}(r)\rho_{\mathrm{v}mn}^{+j+1}]=0 \quad (3)$$

where A is function of the frequency ω. Finally a set of equations is established by combining all of these interfaces and the boundary conditions. And because of the orthogonality of the radial eigenfunctions, these equations can be written in the following form:

$$\begin{bmatrix}\boldsymbol{C}_1 & \boldsymbol{0} & \cdots & \boldsymbol{0}\\ \boldsymbol{0} & \boldsymbol{C}_2 & \cdots & \boldsymbol{0}\\ \vdots & \vdots & & \vdots\\ \boldsymbol{0} & \boldsymbol{0} & \cdots & \boldsymbol{C}_n\end{bmatrix}\begin{bmatrix}\boldsymbol{P}^1\\ \boldsymbol{P}^2\\ \vdots\\ \boldsymbol{P}^n\end{bmatrix}=\boldsymbol{CP}=\boldsymbol{0} \quad (4)$$

where $\boldsymbol{C}_1$, $\boldsymbol{C}_2$, ⋯, $\boldsymbol{C}_n$ are sub matrices and the subscripts denote radial mode number. These sub matrices contain one unknown parameters: the oscillation frequency ω. It can be obtained by solving Eq.(4). The sub matrices of a certain radius mode number n are also independent from others, so the frequency for each mode number can be solved respectively, which can largely simplify our calculations. But it should be noticed that the theory is based on the rigid wall boundary conditions.

Some numerical results are obtained to be compared with either analytical or numerical solutions. Acoustic fields in a duct with an axial temperature gradient are obtained with this theory and they are compared with the exact solutions given by R. I. Sujith, et al[13]. We can see the results agree well (see Fig.3). In Fig.3, T_1 is temperature of left hand of the duct and m the temperature gradient coefficient. The points are results of present theory and lines are results given by Ref.[12].

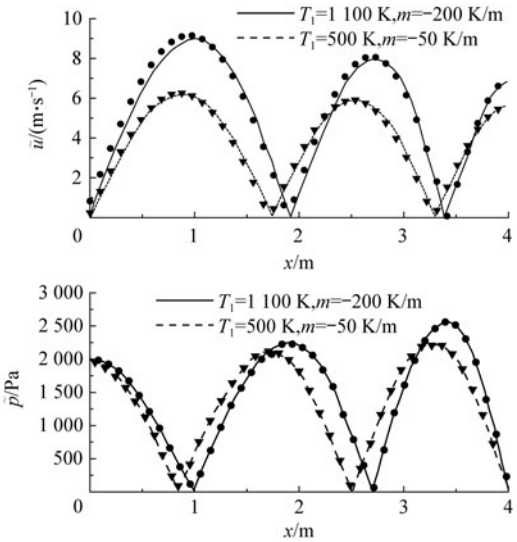

Fig.3 Variation of acoustic pressure amplitude with axial distance in a duct closed at one end and open at the other.

However, the analytical model introduced above cannot be applied to our experiments directly for the central bluff body between the premixed section and the combustor. And it is also inaccurate to give a boundary condition at the break section. Here we use the method developed by R. J. Alfredson[14], which is used for the sound propagation in continuously varying cross-sectional area duct. For low frequency oscillation, there would be only plane wave propagating in the duct, so we treat annulus shape surrounding the central bluff body as a duct of the same area. Next some simple steps will be introduced (see Fig.4).

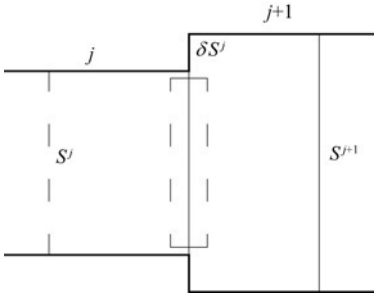

Fig.4 Break section.

For a break section duct, at the interface, we have

the conservation law of mass as the following form:

$$(\rho_0^j u^j + \rho^j U^j)S^j - (\rho_0^{j+1} u^{j+1} + \rho^{j+1} U^{j+1})S^j = 0 \quad (5)$$

where u is the perturbation velocity and U the mean velocity in the duct.

Because at the position δS^j, it is approximate that $u^{j\delta}$=0. After the derivation, we obtain that

$$\sum_{n=1}^{\infty}[A_{mn}^{+j}\psi_{mn}^{+j}(r)P_{mn}^{+j} + A_{mn}^{-j}\psi_{mn}^{-j}(r)P_{mn}^{-j} + A_{vmn}^{+j}\psi_{vmn}^{+j}(r)\rho_{vmn}^{+j} + A_{mn}^{+j+1}\psi_{mn}^{+j+1}(r)P_{mn}^{+j+1} + A_{mn}^{-j+1}\psi_{mn}^{-j+1}(r)P_{mn}^{-j+1} + A_{vmn}^{+j+1}\psi_{vmn}^{+j+1}(r)\rho_{vmn}^{+j+1}] = 0 \quad (6)$$

We should note that it is different for Eq.(6) and Eq.(3). In Eq.(6), the eigenfunction $\psi_{mn}^{+j}(r)$ is different from $\psi_{mn}^{+j+1}(r)$ for two different radii. For plane wave, Eq.(6) is multiplied by r and then integrated from 0 to r_j:

$$A_{01}^{+j}P_{01}^{+j}\int_0^{r_j} r\mathrm{d}r + A_{01}^{-j}P_{01}^{-j}\int_0^{r_j} r\mathrm{d}r + A_{v01}^{+j}\rho_{v01}^{+j}\int_0^{r_j} r\mathrm{d}r + \sum_{n=2}^{N}[A_{mn}^{+j}P_{mn}^{+j}\int_0^{r_j} r\psi_{mn}^{j}(r)\mathrm{d}r + A_{mn}^{-j}P_{mn}^{-j}\int_0^{r_j} r\psi_{mn}^{j}(r)\mathrm{d}r + A_{vmn}^{+j}\rho_{vmn}^{+j}\int_0^{r_j} r\psi_{mn}^{j}(r)\mathrm{d}r] + A_{01}^{+j+1}P_{01}^{+j+1}\int_0^{r_j} r\mathrm{d}r + A_{01}^{-j+1}P_{01}^{-j+1}\int_0^{r_j} r\mathrm{d}r + A_{v01}^{+j+1}\rho_{v01}^{+j+1}\int_0^{r_j} r\mathrm{d}r + \sum_{n=2}^{N}[A_{mn}^{+j+1}P_{mn}^{+j+1}\int_0^{r_j} r\psi_{mn}^{j+1}(r)\mathrm{d}r + A_{mn}^{-j+1}P_{mn}^{-j+1}\int_0^{r_j} r\psi_{mn}^{j+1}(r)\mathrm{d}r + A_{vmn}^{+j+1}\rho_{vmn}^{+j+1}\int_0^{r_j} r\psi_{mn}^{j+1}(r)\mathrm{d}r] = 0 \quad (7)$$

At the position δS^j, we have $\rho_0^{j+1}u^{j+1}$=0. Plusing this with Eq.(7) yields

$$Ab_{101}^{+j}P_{01}^{+j} + Ab_{101}^{-j}P_{01}^{-j} + Ab_{v101}^{+j}\rho_{v01}^{+j} + \sum_{n=2}^{N}(Ab_{10n}^{+j}P_{0n}^{+j} + Ab_{10n}^{-j}P_{0n}^{-j} + Ab_{v10n}^{+j}\rho_{v0n}^{+j}) + Ab_{101}^{+j+1}P_{01}^{+j+1} + Ab_{101}^{-j+1}P_{01}^{-j+1} + Ab_{v101}^{+j+1}\rho_{v01}^{+j+1} + \sum_{n=2}^{N}(Ab_{10n}^{+j+1}P_{0n}^{+j+1} + Ab_{10n}^{-j+1}P_{0n}^{-j+1} + Ab_{v10n}^{+j+1}\rho_{v0n}^{+j+1}) = 0 \quad (8)$$

where Ab_{10n} is the coefficient containing A and the integration about ψ, and in the subscript 10n, the first "1" means the integration function "r", "0" means m=0, "n" means the radius modes. Eq.(6) can also be multiplied by $r\psi_{mn}^{j}(r)$ and be derived by the same steps, so for radius mode number n, we can obtain n equations.

The equation above is obtained from mass continuity relationship. For momentum continuity and energy continuity, we can also get two more equations of the same forms as Eq.(8) after the same steps. Then for one more section, there would be 3n more equations and 3n more unknowns. For example, for n=2 and the section shown in Fig.4, we have

$$\begin{bmatrix} \boldsymbol{Ab}^j & \boldsymbol{Ab}^{j+1} \\ \boldsymbol{Bb}^j & \boldsymbol{Bb}^{j+1} \\ \boldsymbol{Cb}^j & \boldsymbol{Cb}^{j+1} \end{bmatrix} \begin{bmatrix} \boldsymbol{P}^j \\ \boldsymbol{P}^{j+1} \end{bmatrix} \quad (9)$$

where $\boldsymbol{Ab}$, $\boldsymbol{Bb}$ and $\boldsymbol{Cb}$ represent coefficients of mass equation, momentum equation and energy equation, respectively. And they have the following forms:

$$\boldsymbol{Ab}^j = \begin{bmatrix} Ab_{101}^{+j} & Ab_{101}^{-j} & Ab_{v101}^{+j} & Ab_{102}^{+j} & Ab_{102}^{-j} & Ab_{v102}^{+j} \\ Ab_{201}^{+j} & Ab_{201}^{-j} & Ab_{v201}^{+j} & Ab_{202}^{+j} & Ab_{102}^{-j} & Ab_{v102}^{+j} \end{bmatrix} \quad (10)$$

$$\boldsymbol{Bb}^j = \begin{bmatrix} Bb_{101}^{+j} & Bb_{101}^{-j} & Bb_{v101}^{+j} & Bb_{102}^{+j} & Bb_{102}^{-j} & Bb_{v102}^{+j} \\ Bb_{201}^{+j} & Bb_{201}^{-j} & Bb_{v201}^{+j} & Bb_{202}^{+j} & Bb_{102}^{-j} & Bb_{v102}^{+j} \end{bmatrix} \quad (11)$$

$$\boldsymbol{Cb}^j = \begin{bmatrix} Cb_{101}^{+j} & Cb_{101}^{-j} & Cb_{v101}^{+j} & Cb_{102}^{+j} & Cb_{102}^{-j} & Cb_{v102}^{+j} \\ Cb_{201}^{+j} & Cb_{201}^{-j} & Cb_{v201}^{+j} & Cb_{202}^{+j} & Cb_{102}^{-j} & Cb_{v102}^{+j} \end{bmatrix} \quad (12)$$

$$\boldsymbol{P}^j = \begin{bmatrix} P_{01}^{+j} & P_{01}^{-j} & \rho_{v01}^{+j} & P_{02}^{+j} & P_{02}^{-j} & \rho_{v02}^{+j} \end{bmatrix} \quad (13)$$

$\boldsymbol{Ab}^{j+1}$, $\boldsymbol{Bb}^{j+1}$, $\boldsymbol{Cb}^{j+1}$, $\boldsymbol{P}^j$ have the same forms. Eq.(9) is only for one section. To our experiments, there should be another break section, the equations for which have the same form as Eq.(9). Putting equations of these two parts together with other sections and the boundary conditions, the whole analytical model for rigid combustor is built.

4. Some Results for Rigid Wall Combustor

Before the calculation for experiments, a problem should be considered, that is the heat release model. It is difficult for us to give an accurate expression for the unsteady heat release rate of a premixed flame in our experiments. It would be concerned with the fuel rate, the air flow, and the shape of the flame. Here we used a simple model given by A. P. Dowling[15]:

$$Q'(t) = kc_p(T_2 - T_1)\rho_1 u_1'(t-\tau) \quad (14)$$

where T is the temperature, ρ the density, subscripts "2" and "1" denote the parameters after or before the flame; the coefficient k and the time delay τ depend on the frequency. They are also very important parameters in the model. Under most conditions, k varies between 0 and 1.0. The time delay τ is also hard to fix. If the unsteady heat release is brought by fuel rate fluctuation, then its value would be the fuel-convection time from fuel-injection point to the flame. In our experimental setup, the distance from the fuel-injection point to the flame is 1.3 m, which is too large for confirming the convection time. What's more, we have put the fuel-injection before the sonic air inlet and the experimental results change little, so it is evident that the fuel

fluctuation is not the exclusive factor of the unsteady heat input. In the analytical model, all of the real frequency and the imaginary part of frequency would vary with τ, which sometimes would change the instabilities of the system. A. P. Dowling, et al. investigated the relationship of frequency and the growth rate (imaginary part of frequency) with the time delay τ[16]. In our model, we first choose one value, and then some results can be obtained. After comparing with the experimental results, whether the value is reasonable or not would be conformed. But it has to be pointed out that either the value τ or k may not be the right one for our experiments. Fortunately our ultimate aim is to investigate the effect of the perforated liner on the instabilities. So as long as the value of τ or k is reasonable, the law we obtained for the perforated liner would be correct. Table 1 gives details of the geometry we used for our analytical model.

Table 1 Geometry of analytical model

Parameter	Value
Equivalence ratio	0.6
Choked inlet, mass flow rate/(g·s^{-1})	16
Temperature of premixed gas/K	300
Radius of premixed section/m	0.04
Length of premixed section/m	1.5
Radius of break section/m	0.013 2
Length of break section/m	0.1
Time delay/s	0.005 5
Length of combustor/m	0.54
Temperature after combustion/K	2 000

Using parameters given above, some calculated results are shown in Fig.5. The circles in the figure denote the resonant modes of the system for k=0. We can see that almost all of them are positive or very closed to zero, which denote that the modes are stable, because there is no unsteady heat release. When k>0, the unstable modes are near 110, 275, 450 Hz. Generally speaking, these unstable modes would not appear in experiments at a time, because there would not be enough unstable energy. In our experiments we can observe one or two unstable modes and infrequent three. Some experimental results of rigid wall combustor are given in Fig.6. The effective sound pressure and the resonant frequencies of combustor/premixed section as function of the fuel equivalence ratio are shown. For one value of equivalence ratio, there are three repeated experimental results. The resonant frequencies vary from 270 to 300 Hz. In Fig.5 there are unstable modes near 270 Hz. Then we obtained the mode shapes for k=1.0 at this frequency, which are shown in Fig.7. We can see that there are 1.25 m wavelengths in premixed part and 0.5 m wavelength in the combustor. $|p'|$ denotes amplitude of sound pressure. Actually, there will be different mode shapes for every mode and we just paint one which is closed to our experiments. A. P. Dowling, et al. have given all of the mode shapes from 0 to 500 Hz[16].

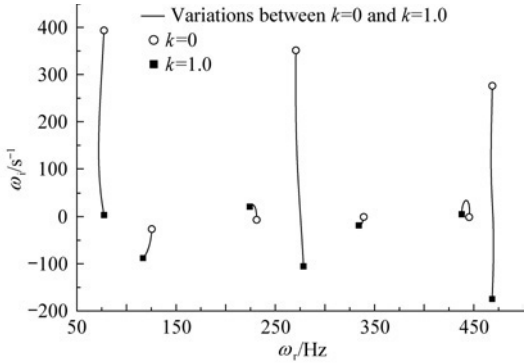

Fig.5 Resonant frequencies by analytical model.

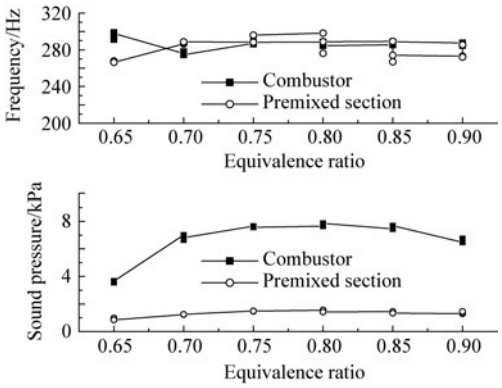

Fig.6 Effective frequency and sound pressure with equivalence ratio obtained in experiments.

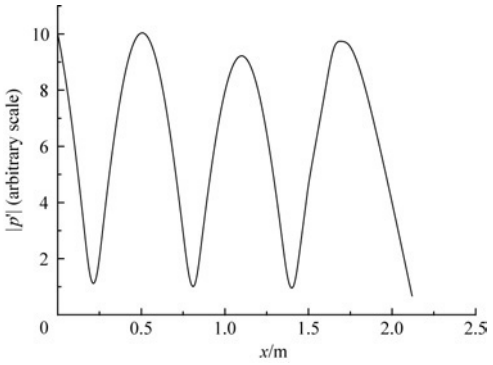

Fig.7 Mode shapes of 278 Hz for k=1.0.

5. Construction of a Transfer Element for a Perforated Liner

Three forms perforated liners have been investigated by J. D. Eldredge, et al.[6]. They are open exterior, annular cavity enclosed by rigid wall and annular cavity enclosed by the second liner. The second form is investigated here for its simple configuration. As shown in Fig.8 the main parameters include the cavity depth r_b, the thickness of perforated plate r_p, the radius of aperture r_a, the space between apertures d and the length of perforated liner l_p.

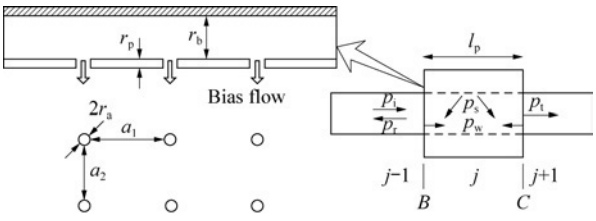

Fig. 8 Configuration of perforated liner in a tube.

As a distributed parameters system, it cannot be modeled in the same way as the Helmholtz resonator. As soft wall boundary condition the 3D thermoacoustic model is needed. But there are still a lot of difficulties here if we solve this problem directly. For rigid wall in a annular duct, the boundary condition can be described by

$$\left.\frac{\partial \tilde{p}}{\partial r}\right|_{r=r_h, r=r_t} = 0 \tag{15}$$

where r_h and r_t denote hub radius and tip radius, respectively. r_h=0 is for the condition of circular duct. Then the eigenvalue k_{mn} can be obtained by solving the equation:

$$J'_m(k_{mn}r_h)Y'_m(k_{mn}r_t) - J'_m(k_{mn}r_t)Y'_m(k_{mn}r_h) = 0 \tag{16}$$

where J_m and Y_m are the first kind and the second kind Bessel function, respectively. It is evident that eigenvalues k_{mn} are only related to r_h and r_t for rigid wall boundary condition. But for the liner section, the wall impedance is a function of the frequency ω, which can be described as $Z=Z(\omega)$. For the relationship between eigenvalues k_{mn} and the wall impedance Z, the eigenvalues would change with the frequency. We conclude that, at least two iteration calculation processes are needed in order to solve the whole problem, as shown in Fig.9. In fact, the "double iteration" numerical process is unstable, and sometimes can not get correct results. To solve this problem, X. F. Sun, et al. developed "transfer element method (TEM)" based on equivalent surface source (ESS) method[11-12].

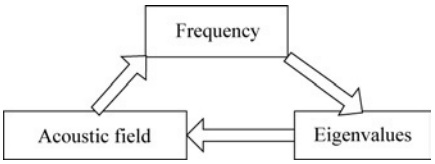

Fig.9 Calculation process with soft wall boundary condition.

In the TEM, the acoustic pressure in the channel can be regarded as a sum of an undisturbed incident acoustic pressure component p_i and a disturbance pressure component p_s:

$$p = p_i + p_s \tag{17}$$

The incident sound pressure p_i is defined as the pressure that would be realized if the lined wall is replaced by a rigid surface. And, on the surface of the perforated plate, the normal component of fluid particle displacement is not zero, so it can be represented by a surface of mass source singularities. Then the disturbance pressure p_s can be generated by this disturbance source. Details of this method have been given in Ref.[12], so we just give the final forms of the total pressure:

$$p = P_w^+ + P_w^- + p_s = \sum_{n=1}^{\infty}\psi_{mn}(r)\sum_{\mu=1}^{\infty}(P_{m\mu}^{+j}p_{\mu n}^{+} + P_{m\mu}^{-j}p_{\mu n}^{-})e^{im\theta} \tag{18}$$

Then all of the acoustic velocity and density could be obtained in the same forms and by now the acoustic field inside the cell has been obtained. Then, the continuity of mass, momentum, energy equations can be written in the following form. At the interface B:

$$\sum_{n=1}^{\infty}[A_{mn}^{+j-1}\psi_{mn}^{+j-1}(r)P_{mn}^{+j-1} + A_{mn}^{-j-1}\psi_{mn}^{-j-1}(r)P_{mn}^{-j-1} + A_{vmn}^{+j-1}\psi_{vmn}^{+j-1}(r)\rho_{vmn}^{+j-1} + \psi_{mn}^{+j}(r)\sum_{\mu=1}^{\infty}A_{mn\mu}^{+j}P_{m\mu}^{+j} + \psi_{mn}^{-j}(r)\sum_{\mu=1}^{\infty}A_{mn\mu}^{-j}P_{m\mu}^{-j} + A_{vmn}^{+j}\psi_{vmn}^{+j}(r)\rho_{vmn}^{+j}] = 0 \tag{19}$$

The equations of interface C have the same forms as Eq.(19). Finally, a set of equations is established by combing these equations, the equations of other parts, the equations of boundary conditions and the equation of heat release model. Noting that eigenfunction $\psi_{mn}(r)$ is orthogonal for n=1, 2, …, N, after the orthogonal transform, we can obtain closed equations for unknown variable P_{mn}. For the rigid wall part, every radius mode is independent from others. But for the liner part, all radius modes are tangled, which brings troubles to work of solution. Fortunately our purpose is to study low order modes, and it is accurate enough for a small truncated number $\mu=N_\mu$. As shown in Fig.8, for the part $j-1, j, j+1$, we give the equation for N_μ=2.

$$\begin{bmatrix} \boldsymbol{D}_{11} & \boldsymbol{D}_{12} & \boldsymbol{0} \\ \boldsymbol{0} & \boldsymbol{D}_{22} & \boldsymbol{D}_{23} \end{bmatrix}\begin{bmatrix} \boldsymbol{P}_1 \\ \boldsymbol{P}_2 \\ \boldsymbol{P}_3 \end{bmatrix} = \boldsymbol{0} \tag{20}$$

where sub matrixes $\boldsymbol{D}$ and $\boldsymbol{P}$ are as the following forms:

$$\boldsymbol{D}_{11} = \begin{bmatrix} A_{m1}^{+j-1} & A_{m1}^{-j-1} & A_{vm1}^{+j-1} & 0 & 0 & 0 \\ B_{m1}^{+j-1} & B_{m1}^{-j-1} & B_{vm1}^{+j-1} & 0 & 0 & 0 \\ C_{m1}^{+j-1} & C_{m1}^{-j-1} & C_{vm1}^{+j-1} & 0 & 0 & 0 \\ 0 & 0 & 0 & A_{m2}^{+j-1} & A_{m2}^{-j-1} & A_{vm2}^{+j-1} \\ 0 & 0 & 0 & B_{m2}^{+j-1} & B_{m2}^{-j-1} & B_{vm2}^{+j-1} \\ 0 & 0 & 0 & C_{m2}^{+j-1} & C_{m2}^{-j-1} & C_{vm2}^{+j-1} \end{bmatrix}$$

$$\boldsymbol{D}_{12} = \begin{bmatrix} A_{Lm11}^{+j} & A_{Lm11}^{-j} & A_{Lvm12}^{+j} & A_{Lm12}^{+j} & A_{Lm12}^{-j} & 0 \\ B_{Lm11}^{+j} & B_{Lm11}^{-j} & B_{Lvm1}^{+j} & B_{Lm12}^{+j} & B_{Lm12}^{-j} & 0 \\ C_{Lm11}^{+j} & C_{Lm11}^{-j} & C_{Lvm1}^{+j} & C_{Lm12}^{+j} & C_{Lm12}^{-j} & 0 \\ A_{Lm21}^{+j} & A_{Lm21}^{-j} & 0 & A_{Lm22}^{+j} & A_{Lm22}^{-j} & A_{Lvm22}^{+j} \\ B_{Lm21}^{+j} & B_{Lm21}^{-j} & 0 & B_{Lm22}^{+j} & B_{Lm22}^{-j} & B_{Lvm22}^{+j} \\ C_{Lm21}^{+j} & C_{Lm21}^{-j} & 0 & C_{Lm22}^{+j} & C_{Lm22}^{-j} & C_{Lvm22}^{+j} \end{bmatrix}$$

$$\boldsymbol{D}_{22}=\begin{bmatrix} A^{+j}_{Rm11} & A^{-j}_{Rm11} & A^{+j}_{Rvm12} & A^{+j}_{Rm12} & A^{-j}_{Rm12} & 0 \\ B^{+j}_{Rm11} & B^{-j}_{Rm11} & B^{+j}_{Rvm1} & B^{+j}_{Rm12} & B^{-j}_{Rm12} & 0 \\ C^{+j}_{Rm11} & C^{-j}_{Rm11} & C^{+j}_{Rvm1} & C^{+j}_{Rm12} & C^{-j}_{Rm12} & 0 \\ A^{+j}_{Rm21} & A^{-j}_{Rm21} & 0 & A^{+j}_{Rm22} & A^{-j}_{Rm22} & A^{+j}_{Rvm22} \\ B^{+j}_{Rm21} & B^{-j}_{Rm21} & 0 & B^{+j}_{Rm22} & B^{-j}_{Rm22} & B^{+j}_{Rvm22} \\ C^{+j}_{Rm21} & C^{-j}_{Rm21} & 0 & C^{+j}_{Rm22} & C^{-j}_{Rm22} & C^{+j}_{Rvm22} \end{bmatrix}$$

$$\boldsymbol{D}_{23}=\begin{bmatrix} A^{+j+1}_{m1} & A^{-j+1}_{m1} & A^{+j+1}_{vm1} & 0 & 0 & 0 \\ B^{+j+1}_{m1} & B^{-j+1}_{m1} & B^{+j+1}_{vm1} & 0 & 0 & 0 \\ C^{+j+1}_{m1} & C^{-j+1}_{m1} & C^{+j+1}_{vm1} & 0 & 0 & 0 \\ 0 & 0 & 0 & A^{+j+1}_{m2} & A^{-j+1}_{m2} & A^{+j+1}_{vm2} \\ 0 & 0 & 0 & B^{+j+1}_{m2} & B^{-j+1}_{m2} & B^{+j+1}_{vm2} \\ 0 & 0 & 0 & C^{+j+1}_{m2} & C^{-j+1}_{m2} & C^{+j+1}_{vm2} \end{bmatrix}$$

$$\boldsymbol{\rho}_1=[P^{+j-1}_{m1}\quad P^{-j-1}_{m1}\quad \rho^{+j-1}_{vm1}\quad P^{+j-1}_{m2}\quad P^{-j-1}_{m2}\quad \rho^{+j-1}_{vm2}]^{\mathrm{T}}$$

$$\boldsymbol{\rho}_2=[P^{+j}_{m1}\quad P^{-j}_{m1}\quad \rho^{+j}_{vm1}\quad P^{+j}_{m2}\quad P^{-j}_{m2}\quad \rho^{+j}_{vm2}]^{\mathrm{T}}$$

$$\boldsymbol{\rho}_3=[P^{+j+1}_{m1}\quad P^{-j+1}_{m1}\quad \rho^{+j+1}_{vm1}\quad P^{+j+1}_{m2}\quad P^{-j+1}_{m2}\quad \rho^{+j+1}_{vm2}]^{\mathrm{T}}$$

where A, B and C are parameters in mass, momentum, energy equations, respectively. $\boldsymbol{D}_{11}$ is for the interface B in part $j-1$, $\boldsymbol{D}_{12}$ is for the interface B in part j, $\boldsymbol{D}_{22}$ is for the interface C in part j, and $\boldsymbol{D}_{23}$ is for the interface C in part $j+1$.

Then, together with equations of other parts, the resonance frequency can be calculated.

6. Experimental and Analytical Results

We have investigated the effects of perforated liners for two different parameters (see Table 2). The liner is fixed at the place 110 mm away from central bluff body. The aperture radius is 1 mm. And there are two air-inlet holes on the outer wall surface, which are used for rising bias flows at the apertures in inner wall.

Table 2 Details of perforated liner

Number	Length/mm	Opening ratio	Cavity depth /mm
1#	80	0.020 2	60
2#	80	0.037 5	60

Fig.10 shows the effect of 1# liner on unstable growth rate for the resonating frequency near 270 Hz, for k from 0.5 to 1.0. The calculations are based on parameters used above. In calculation we are only aimed at the frequency near 270 Hz, because it is the dominating fluctuation frequency in experiments. Four different lines denote four different bias flow Mach numbers. The left points on every line are for k=0.5 and the right side for k=1.0. And other points on lines denote values for k from 0.6 to 0.9. To some extent, the varying of k can reflect the effects of equivalence ratio changing in experiments. Compared to the rigid wall, the growth rate decreases a little when there is perforated liner in system. Fig.11 shows experimental results. We can see that with the perforated liner, the maximum effective sound pressure depresses from 8 kPa to 5 kPa. From Figs.10-11, we also find that the existence of bias flow almost has nothing to do with improving control effect. But other works have pointed out that the bias flow could enhance the damping of sound energy[6-7]. Maybe it is because that in the combustion system the unstable energy is so large that the added damping by bias flow could be ignored. In addition, we can give any bias flow Mach number in the calculation arbitrarily, but it is difficult to get the accurate Mach number in the perforated plate in experiments for the lack of temperature information of air flow in back chamber. So we have to estimate the Mach numbers as 0.01 and 0.02, when practical air flow are 5 m^3/h and 10 m^3/h.

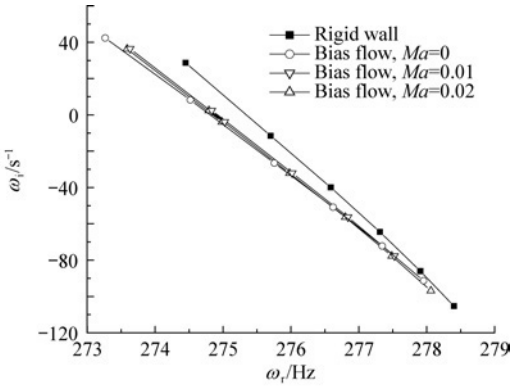

Fig.10 Effect of 1# liner on unstable growth rate for frequency near 270 Hz.

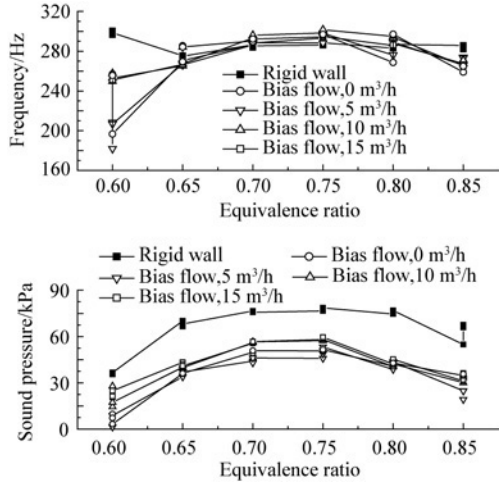

Fig.11 Effective frequency and sound pressure with effect of 1# liner.

In Figs.12-13 there are some results of 2# liner. It is the same as 1#, for calculated results, the growth rate decreases a little with the effect of liner. But in experiments the maximum effective sound pressure decreases from 8 kPa to 2 kPa, which denotes that the control effect of 2# is better than 1#. It is because that 2# liner has larger open ratio (from 0.037 5 to

0.020 2).

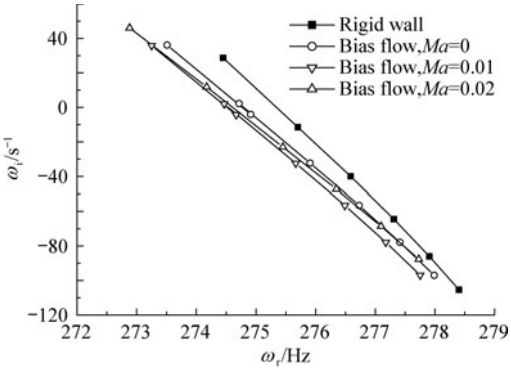

Fig.12 Effect of 2# liner on unstable growth rate for frequency near 270 Hz.

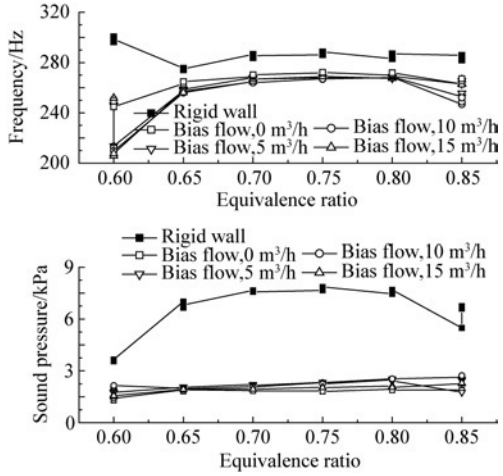

Fig.13 Effective frequency and sound pressure with effect of 2# liner.

7. Conclusions

Experiments of simple premixed prevaporised methane-fueled combustor are set up. In experiments the large oscillations occur when equivalence ratio changes from 0.6 to 0.9. The perforated liner is used for damping the instabilities. Then an analytical 3D model, with the effect of perforated liner and the heat release model, is established. From experimental data and the computational results, we find the instabilities could be largely suppressed by the perforated liners. And the existence of bias flow in back chamber of the liner has little effect on enhancing the control effect. By comparison of experimental and computational results, it is found that the analytical model can predict the instabilities of the system. However, it is not accurate under some conditions. Furthermore improvement to the model is required to extend its application range.

References

[1] Zinn B T, Lieuwen T C. Combustion instabilities: basic concepts. In: Lieuwen T C, Yang V, editors. Combustion Instabilities in Gas Turbine Engines: Operational Experience, Fundamental Mechanisms, and Modeling. Reston, VA: AIAA, 2005; 3-28.

[2] Heckl M A. Active control of the noise from a rijke tube. Journal of Sound and Vibration 1988; 124(1): 117-133.

[3] Uhm J H, Acharya S. Control of combustion instability with a high-momentum air jet. Combustion and Flame 2004; 139(1-2): 106-125.

[4] Dupere I D J, Dowling A P. The use of Helmholtz resonators in a practical combustor. Journal of Engineering for Gas Turbines and Power 2005; 127(2): 268-275.

[5] Zhao D, Morgans A S. Tuned passive control of combustion instabilities using multiple Helmholtz resonators. Journal of Sound and Vibration 2009; 320(4-5): 744-757.

[6] Eldredge J D, Dowling A P. The absorption of axial acoustic waves by perforated liner with bias flow. Journal of Fluid and Mechanics 2003; 485: 307-335.

[7] Jing X D, Sun X F. Experimental investigations of perforated liners with bias flow. Journal of Acoustic Society of America 1999; 106(5): 2436-2441.

[8] Jing X D, Sun X F. Effect of plate thickness on impedance of perforated plates with bias flow. AIAA Journal 2000; 38(9): 1573-1578.

[9] Eldredge J D. On the interaction of higher duct modes with a perforated liner system with bias flow. Journal of Fluid and Mechanics 2004; 510: 303-331.

[10] You D N, Yang V, Sun X F. Three-dimensional linear stability analysis of gas turbine combustion dynamics. In: Lieuwen T C, Yang V, editors. Combustion Instabilities in Gas Turbine Engines: Operational Experience, Fundamental Mechanisms, and Modeling. Reston VA: AIAA 2005; 415-442.

[11] Namba M, Fukushige K. Application of the equivalent surface source method to the acoustics of duct systems with non-uniform wall impedance. Journal of Sound and Vibration 1980; 73(1): 125-146.

[12] Sun X F, Wang X Y, Du L, et al. A new model for the prediction of turbofan noise with the effect of locally and non-locally reacting liners. Journal of Sound and Vibration 2008; 316(1-5): 50-68.

[13] Sujith R I, Waldherr G A, Zinn B T. An exact solution for one-dimensional acoustic fields in ducts with an axial temperature gradient. Journal of Sound and Vibration 1995; 184(3): 389-402.

[14] Alfredson R J. The propagation of sound in a circular duct of continuously varying cross-sectional area. Journal of Sound and Vibration 1972; 23(4): 433-442.

[15] Dowling A P. The calculation of thermoacoustic oscillations. Journal of Sound and Vibration 1995; 180(4): 557-581.

[16] Dowling A P, Stow S R. Acoustic analysis of gas-turbine combustors. Journal of Propulsion and Power 2003; 19(5): 751-764.

Biography:

Li Lei Born in 1981, he received his B.E. degree from Beijing University of Aeronautics and Astronautics in 2004, and then became a postgraduate there. His main research interest is combustion instability.
E-mail: Lesanstone@126.com